Outer Raceway Fault Detection and Localization for Deep Groove Ball Bearings by Using Thermal Imaging

Raiko SCHULZ [1,2], Mia LOCCUFIER [2], Steven VERSTOCKT [3],
Kurt STOCKMAN [1], Sofie VAN HOECKE [1,3]

[1] Department of Industrial System and Product Design, Ghent University Campus Kortrijk; Kortrijk, Belgium
Phone: +32 5624 1252, Fax: +32 9264 3594; e-mail: raiko.schulz@ugent.be, kurt.stockman@ugent.be, sofie.vanhoecke@ugent.be
[2] SYSTeMS Research Group, Department of Electrical Energy, Systems and Automation, Ghent University, Ghent, Belgium; e-mail: mia.loccufier@ugent.be
[3] Multimedia Lab, Department of Electronics and Information Systems, Ghent University - iMinds, Ghent, Belgium; e-mail: steven.verstockt@ugent.be

Abstract
This paper discusses outer raceway fault detection and localization for rolling element bearings by means of thermal imaging. In particular, deep groove ball bearings have been monitored. Whereas bearings in industrial applications are usually fully covered, the used test setup allows to monitor the uncovered bearings to understand their heat increase and propagation. The main contribution of this paper is the methodology to process and analyse the thermal data of the bearings. The presented methodology is applied on both a healthy bearing and a bearing with outer raceway fault. By revealing significantly higher temperatures for the faulty bearing than for the healthy bearing, thermal imaging enables fault detection. Additionally, the stationary characteristic of the outer ring allows to locate the outer raceway fault by means of its thermal impact.

Keywords: deep groove ball bearings, passive thermography, thermal imaging, infrared, fault detection, fault localization, non-destructive testing

1. Introduction

Cost-efficient operation of remote industrial machinery such as drive trains of offshore wind turbines has to meet several challenges. Limited accessibility makes maintenance more expensive, requires efficient scheduling and turbine operation to be interrupted for visual inspection by specialist staff. Therefore, a sensor-based real-time condition monitoring is required to keep downtime and maintenance costs low and guarantee energy generation [1, 2]. As multiple sensors are needed to monitor a drive train and their installation requires to stop operation, choosing the right sensor types is crucial. The complexity of drive trains, such as different gearbox configurations or usage of different bearing types in accordance to loading conditions, makes it difficult to develop a global and cost-effective solution [3].

The tribological drive train components such as bearings and gearboxes are naturally affected by friction and wear, causing increased vibrations, acoustic emissions and heat as well as particles that may contaminate the lubricant [4, 5]. Faults in the drive trains, especially in gearbox and bearings, are the main cause for downtime [6, 7]. Bearing failures belong to the major issues in wind turbine drive train reliability, as the bearings must deal with cyclic and transient loading as well as alignment issues [5]. The majority of wind turbine gearbox failures also appear to initiate in the bearings. They may later propagate into the gear teeth because bearing debris and excess clearances cause surface wear and misalignments [8].

Present condition monitoring of industrial machinery may include vibration analysis, acoustic emissions and lubricant analysis. All present techniques still show shortcomings for real-time measurements and data processing [3, 9]. In particular, vibrations and acoustic emissions propagate through the structure which can make fault localization difficult. Other techniques

such as lubricant analysis require onshore sample analysis in order to identify the faulty component, which itself is already costly in terms of time and financing and requires a system stop in order to take probes [10].

Bearings show temperature changes for a variety of faults [11, 12], further raising potential for thermal imaging. To examine the feasibility of thermal imaging for monitoring drive-train components, deep groove ball bearings, which are used in larger size in wind turbine generators to provide current isolation, have been monitored. After discussing the state of the art of thermal imaging on rotating machinery and introducing the used test setup, the remainder of this paper discusses a methodology for processing the thermal data of the bearings. The presented methodology is then applied on both healthy and faulty bearings to discuss and compare their thermal characteristics.

2. State of the art

Thermal imaging already is commonly used on test rigs and also real environments such as pipelines, underground reservoirs and electric components. Monitoring of test rigs and manual inspections in industry are widely performed by active thermography. For active thermography, the target to be monitored gets stimulated by a source of heat or cooling to allow its thermal characteristics to be monitored [13, 14], such as for manual inspection of airplane turbines and composites after landing [15]. Passive thermography for automatic monitoring can be applied if the targets are naturally showing heat increase without the need of further stimulation. In industrial applications, uniform components such as rollers or bearings on conveyor belts affected by friction can be easily monitored for fault detection as well as pipelines or reservoirs for leak detection based on heat loss. As wind turbine drive trains are remote and complex systems, manual inspection is inefficient and costly. Wind turbine drive trains require reliable and automated real-time monitoring. As thermal imaging is a non-contacting and non-intrusive technique, it enables drive train condition monitoring without stopping its operation.

Despite its potential, thermal imaging has not received wide application on rotating machinery yet and requires further research to be established in real-time online condition monitoring [16, 17]. As the same heat increase might be caused for different reasons, the measurements need to be confirmed by another technique such as vibration analysis. In contrast to vibrations, the temperature rise caused by a fault is a more local phenomenon. Furthermore, thermal imaging allows spatial visualization of a monitored area and its heat propagation and therefore can support fault localization based on heat increase in a multi-sensor solution.

3. Experimental setup and procedure

For the tests, the Machinery Fault Simulator Lite[1] by SpectraQuest was used. This setup is schematically shown in Figure 1 and designed to study bearing faults as well as balancing, alignment, resonance, crack shafts, fan and mechanical rub. In particular, this setup allows to directly monitor the inner ring of the bearing whereas the outer ring and the outer part of the seal are covered by the aluminium housing. This allows to receive insight in the thermal behaviour of the bearings which are usually completely covered and sealed in industrial applications. The test setup also includes two rotors to add axial load to the bearings.

[1] http://www.spectraquest.com/machinery-fault-simulator/details/mfs-lt

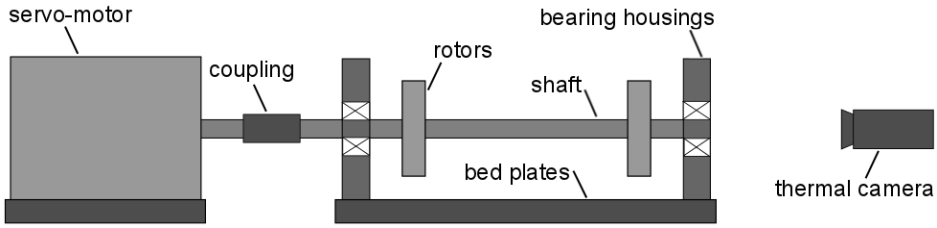

Figure 1. Scheme of Machinery Fault Simulator Lite

ER10K deep groove ball bearings[2] by Rexnord have been used, having an outside diameter of 47.00mm and a shaft diameter of 15.86mm. Figure 2 shows a three-dimensional cross-section of such a bearing, indicating its main parts. The bearing is mounted to the shaft by means of a screw locking. The rolling elements are covered by a single lip seal. The seal protects the rolling elements and raceways from contamination by water or hard-particles but also prohibits a direct monitoring of the rolling elements.

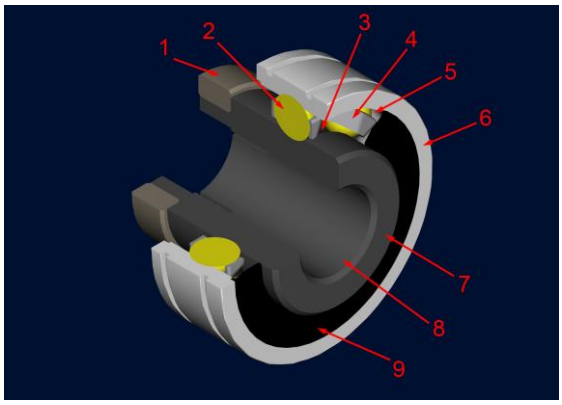

bearing parts	
1	screw locking
2	rolling elements
3	inner raceway
4	cage
5	outer raceway
6	outer ring
7	inner ring
8	inner ring bore
9	single lip seal

Figure 2. 3D scheme of deep groove ball bearing

The bearings have been running at a rotational speed of 1,500 rotations per minute, which is a standard rotational speed for high-speed components of wind turbine drive trains in Europe. The thermal imaging was performed by a FLIR A655sc uncooled long-wave infrared camera[3]. The measurements discussed in this paper focus on the heat increase over time and less on the general impact of the rotational movement. Therefore, the images have been taken at a frame rate of one frame per second.

4. Methodology

Both, healthy and faulty bearings have been monitored by a thermal camera. Before the start of each measurement, the setup was cooled down to ambient temperature. Each measurement has been performed for a period of fifty minutes. Trend analysis is applied as a first step in order to examine the over-time heat increase of the bearing components.

Figure 3 shows a bearing mounted within its housing, schematically indicating the parts that can be monitored from the chosen camera location. The same scheme has been added to the thermal images discussed in this paper to facilitate their interpretability. In order to simplify the comparability of healthy and faulty bearing discussed in this paper, the thermal images are

[2] http://www.rexnord.com/sites/Process/Pages/ProductPage.aspx?platformkey=1&businessunitkey=42&nodekey=161986
[3] http://www.flir.com/thermography/americas/us/view/?id=46802

shown in a fixed relative temperature range. The chosen temperature limits result from the relative minimum temperature of the healthy bearing and the relative maximum temperature of the bearing with outer raceway fault.

As the non-uniform surfaces of the single bearing parts cause differences in the distance to the camera, reading of the thermal measurements has to be performed carefully. The different surfaces show different temperature ranges which can strongly affect statistical features such as mean temperatures. Therefore, the analysis focusses on the *maximum temperatures* of the single bearings parts. In addition, consistent results independent of the ambient temperatures measured by thermocouples, are obtained by using *relative temperatures*. A calibration effect caused by the camera occurred for the original absolute temperatures of both the bearing parts and the thermocouples, and is excluded as well by using the relative temperatures. The resulting trend graphs show the *relative maximum temperatures* of the bearing components, being the differences between the maximum temperatures of the single bearing parts and the ambient temperature. The trends of the single bearing components have been matched with first-order systems to determine their time constants. The time constant of the system response is the time it takes the step response to rise to 63% of its final value [18].

Beside the heat increase over time, the trend graphs reveal individual frames, or thermal images, of interest, for example a steady-state or temperature peaks. For further analysis such as of heat propagation, temperature profiles are created for single frames. Figure 4 shows the directions of the profile lines. In general, both a horizontal and a vertical temperature profile line are added to the thermal image to examine the temperatures of the bearing parts and to compare healthy and faulty bearings. The profile lines are always taken from bottom to top for the vertical profile, and from left to right side for the horizontal profile.

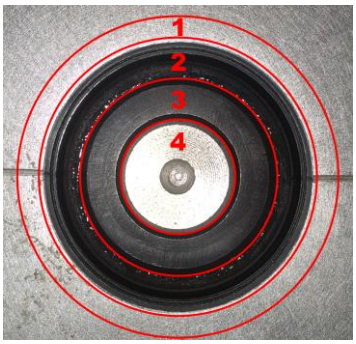

bearing parts	
1	outer ring
2	single lip seal
3	inner ring
4	shaft

Figure 3. Frontal image of mounted deep groove ball bearing with schematic overlay of the bearing parts

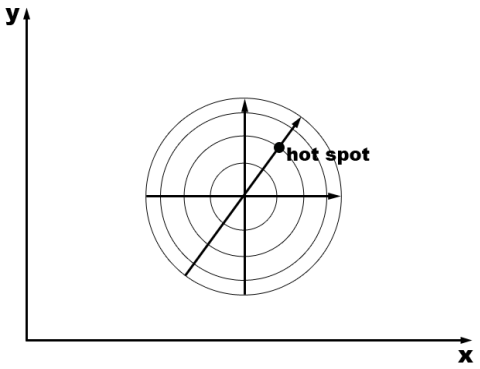

Figure 4. Temperature profile directions

The stationary characteristic of the outer ring can support localization of outer raceway faults. In order to identify hot spots, which indicate potential fault locations, each thermal image of a measurement period has been overlaid with a circle having its diameter matched with the outer bearing diameter. By monitoring the area within the circle, minimum and maximum temperatures can be monitored over time. After detecting a hot spot, which is continuously showing the highest temperature, an additional profile line is added and analysed, passing through the hot spot and the center of shaft and bearing.

5. Thermal characterization of a healthy bearing

The trend graphs in Figure 5 show the relative maximum temperatures for the main parts of the healthy bearing. All graphs start from a temperature higher than the ambient temperature

as the stationary bearing in the beginning is strongly affected by noise effects such as reflection of light. Especially for the inner ring, the impact of reflection of light was observed in non-operating state but became less with heating up of the setup. The highest temperatures occur at the contact surfaces of the inner ring with both shaft and rolling elements. At the end of the measurement period, the maximum temperature is 9.55°C above ambient temperature for the contact surface of inner ring and shaft, and 8.31°C for the contact surface between inner ring and rolling elements.

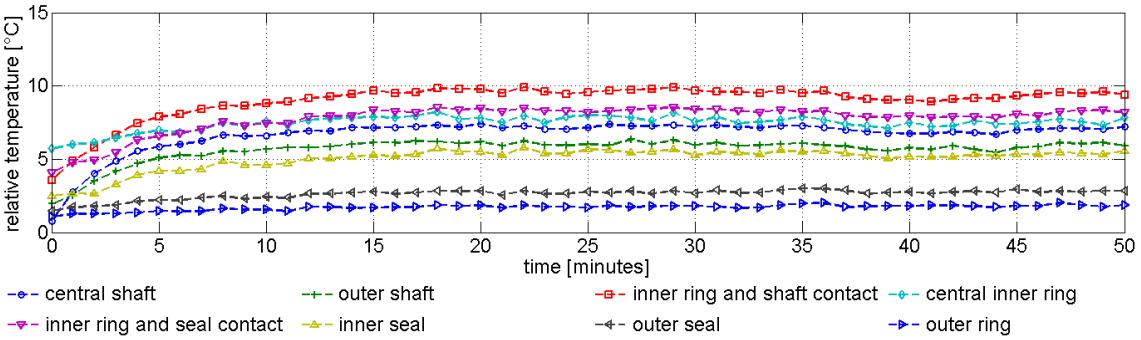

Figure 5. Trend graphs showing the relative maximum temperatures for healthy deep groove ball bearing

Figure 6 shows the thermal image for the healthy bearing with relative temperature scale after fifty minutes. The dark representation results from the maximum temperature limit being increased to the maximum temperature limit of the faulty bearing to support comparison. The single bearing parts such as inner ring and seal can be identified by their different temperatures. As already indicated in the trend graphs, both contact surfaces of the inner ring show the highest temperatures.

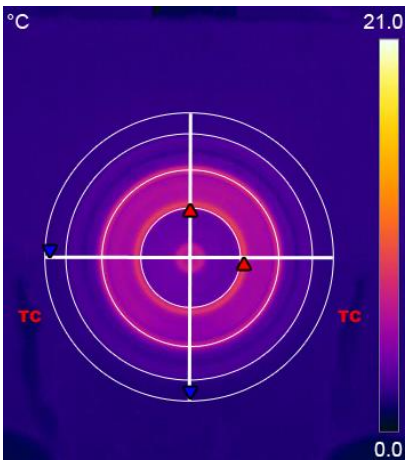

Figure 6. Thermal image of healthy deep groove ball bearing, indicating both vertical and horizontal temperature profile axes and two thermocouples (TC)

For the temperatures of the healthy bearing, a mirror effect in accordance to its symmetry might be expected but different loading and heat transfer conditions in lower and upper bearing have to be considered. The rolling elements are in direct contact with both raceways in the loaded bottom part of the bearing, but they are pushed against the outer ring in the upper unloaded part by centrifugal force. As it is shown in Figure 7, the horizontal profile line shows symmetric characteristics, whereas the vertical profile line reveals slightly higher temperatures for the upper inner ring than for the lower inner ring. Whereas the highest temperatures would be expected at the raceways, a relative maximum temperature of 9.55°C

was measured at the contact surface of the inner ring with the shaft. This part of the healthy bearing consistently showing the highest temperatures may indicate a second origin of heat such as bending of the shaft, propagating from shaft to inner ring. As the shaft sticks out from the bearing for a length of 5mm, the outer shaft part being visible from the chosen camera location is affected by a cooling effect and shows lower temperatures than the contact surface between inner ring and shaft. Additionally, outer shaft and central shaft show significant temperature differences. These temperature differences are caused by a bore-hole in the shaft center which is revealing its inside temperature.

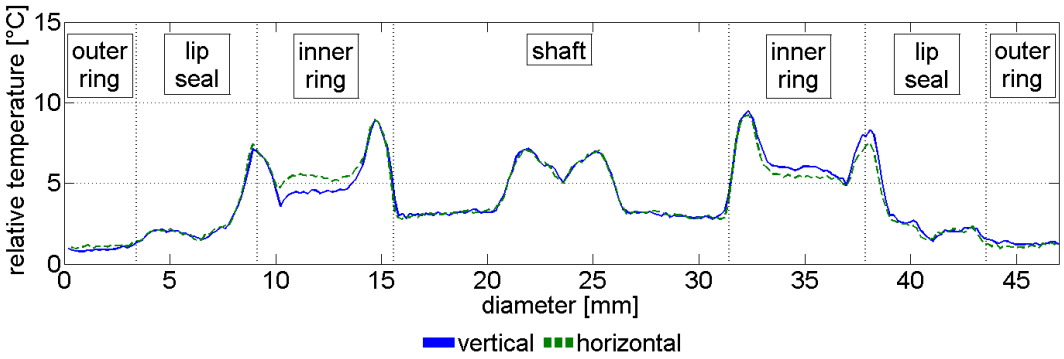

Figure 7. Temperature profiles for the healthy bearing

6. Thermal characterization of a bearing with outer raceway fault

The trend graphs in Figure 8 show the relative maximum temperatures for the bearing with outer raceway fault. The graphs reveal a higher temperature level for the outer raceway fault than for the healthy bearing. In contrast to the healthy bearing, not the contact surface between inner ring and shaft shows the highest temperature over time, but the contact surface between inner ring and rolling elements. Its relative maximum temperature after fifty minutes is 21.03°C. A more in-depth analysis of the heat increase is provided in Section 7, including the time constants of first-order systems that have been matched with the measurements.

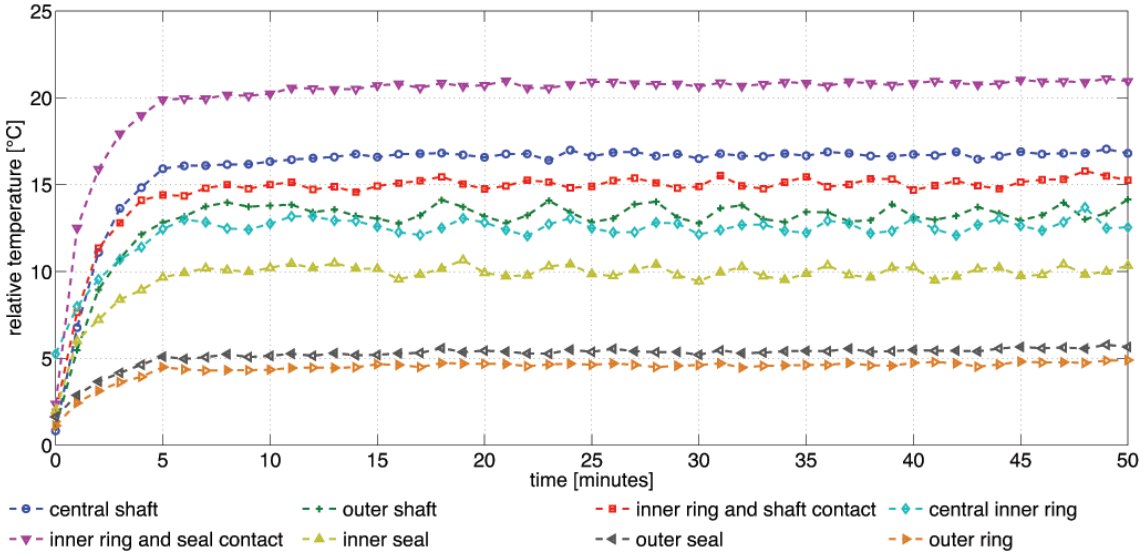

Figure 8. Trend graphs showing the relative maximum temperatures for deep groove ball bearing with outer raceway fault

The thermal image in Figure 9 shows the faulty bearing with relative temperature scale after

fifty minutes. For both the healthy bearing and the outer raceway fault, the same temperature range has been chosen for visualization. The more bright appearance of the faulty bearing in opposition to the healthy bearing reveals an overall higher temperature, as also indicated in the trend graphs. Both horizontal and vertical temperature profiles reveal maximum temperatures in the upper right of the bearing. Therefore, the third profile line is added which marks the hot spot caused by the outer raceway fault to the contact surface between inner ring and rolling elements.

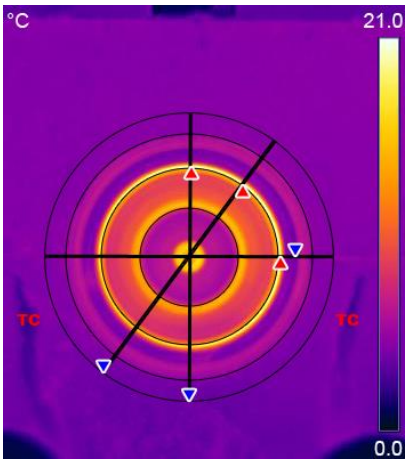

Figure 9. Thermal image of deep groove ball bearing with outer raceway fault, indicating vertical, horizontal and hot spot temperature profile axes as well as two thermocouples (TC)

Figure 10 shows the horizontal and vertical temperature profiles, whereas the hot spot profile is discussed in Section 7. The contact surface between inner ring and rolling elements showing the highest temperatures indicates heat propagation from the faulty outer raceway towards the inner raceway by means of convection, as also stated in [19]. Furthermore, inner ring and shaft show significant increase as well, indicating further heat propagation from the inner raceway towards the shaft by means of conduction. In opposition to the healthy bearing, the temperatures between the housing part covering the outer ring and the lip seal are more distinct. Additionally, the outer lip seal connected to the outer ring shows higher temperatures than the inner lip seal. The temperature profiles show an asymmetric behaviour with higher temperatures on top and at the right half of the bearing.

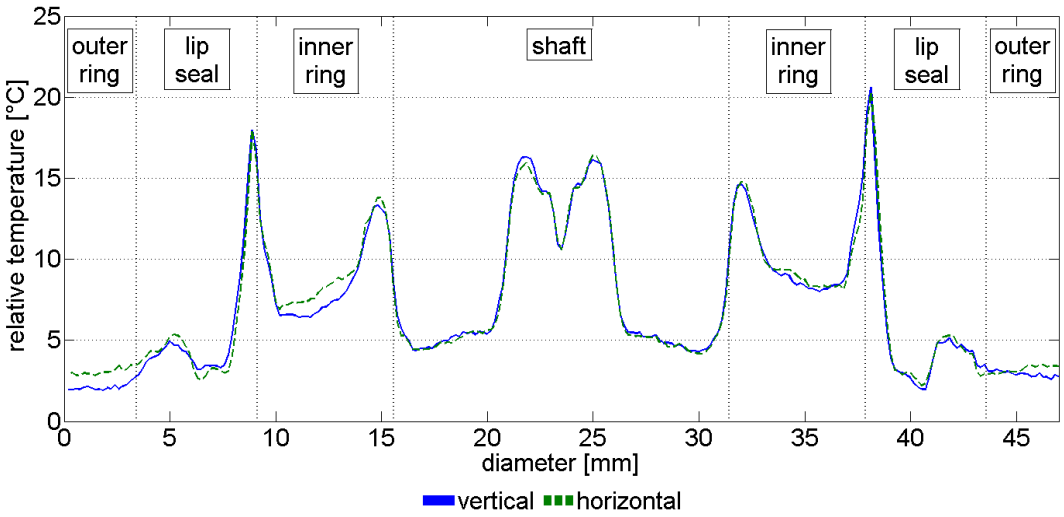

Figure 10. Vertical and horizontal temperature profiles for bearing with outer raceway fault

7. Opportunities for fault detection and localization

The ambient temperature measured by the thermocouples has shown only little differences, being 1.49°C higher for the outer raceway fault test than for the healthy bearing test, whereas the camera accuracy is 1°C. Although the ambient temperature is almost the same, the relative maximum temperatures of the single bearing parts clearly differ for the outer raceway fault and the healthy bearing. In contrast to the healthy bearing, a more distinct temperature difference is shown between the housing part covering the outer ring and the lip seal. Furthermore, the outer raceway fault overall causes the temperatures to rise faster than for the healthy bearing. After fifty minutes, the relative temperature difference between the healthy bearing and the bearing with outer raceway fault is 12.69°C at the contact surface between inner ring and rolling elements, and 2.86°C at the housing part covering the outer ring.

Table 1 shows the time constants for subcomponents of both healthy and faulty bearing. The subcomponents include the contact surface of the inner ring towards the shaft as well as the covered outer ring and show significant difference for both visible and covered components. The hole in the central shaft allows measurements of the actual shaft temperature and is therefore also shown. The time constants clearly indicate a more rapid increase in temperature for the bearing with outer raceway fault than for the healthy bearing.

Table 1. Time constants for subcomponents of both healthy and faulty bearing

bearing	healthy	outer raceway fault
housing part covering the outer ring	8.0	2.4
contact surface of inner ring with shaft	3.9	1.6
central shaft	2.8	2.0

Figure 11 exemplarily shows the matching of the trend graph for the contact surface between inner ring of the healthy deep groove ball bearing and shaft with its first-order step response. The fit of trend graph and step response support the validity of the chosen time constants.

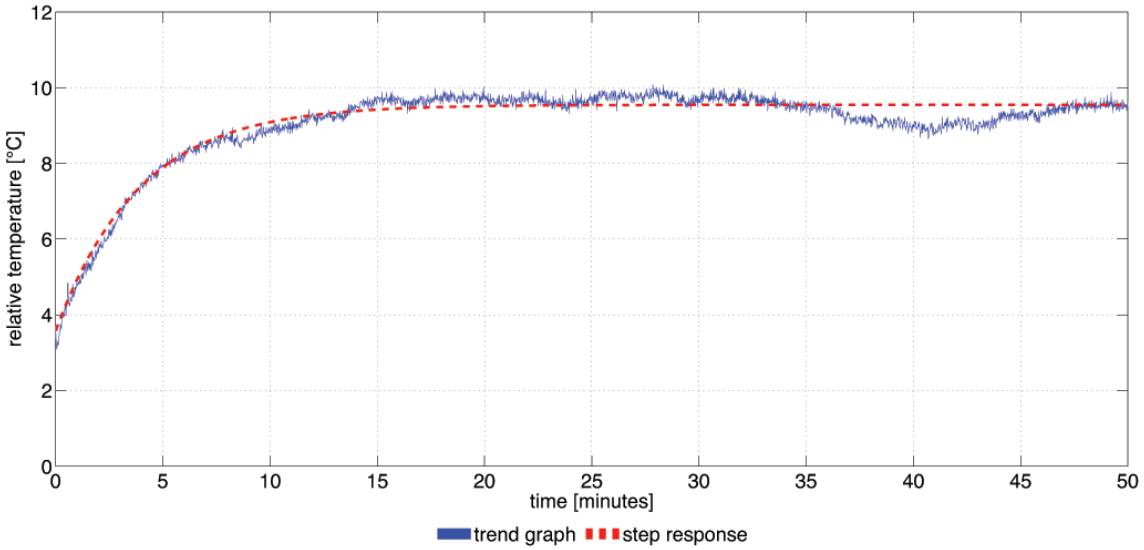

Figure 11. Trend graph and first-order step response for contact surface between inner ring and shaft of healthy deep groove ball bearing

As the temperature rise caused by the outer raceway fault propagates through the rolling elements to the inner raceway, a hotspot occurs in the upper right of the bearing. This hotspot

appears after the starting and heating up process of the setup and remains for the rest of the measurement period. As shown in Figure 9, the hot spot profile line indicates the hot spot with a relative maximum temperature of 21.03°C at the contact surface between inner ring and rolling elements.

The hot spot profile is shown in Figure 12 together with the same profile line taken for the healthy bearing. Both profiles cross the location of the hot spot monitored for the outer raceway fault at the contact surface of inner ring and rolling elements, and show distinct peaks for both contact surfaces of the inner ring. The temperature profile for the bearing with outer raceway fault shows generally higher temperatures than for the healthy bearing, and a significantly higher peak for the upper right of the inner ring than for the lower left side. Increased temperatures also occur for the housing part covering the faulty outer ring.

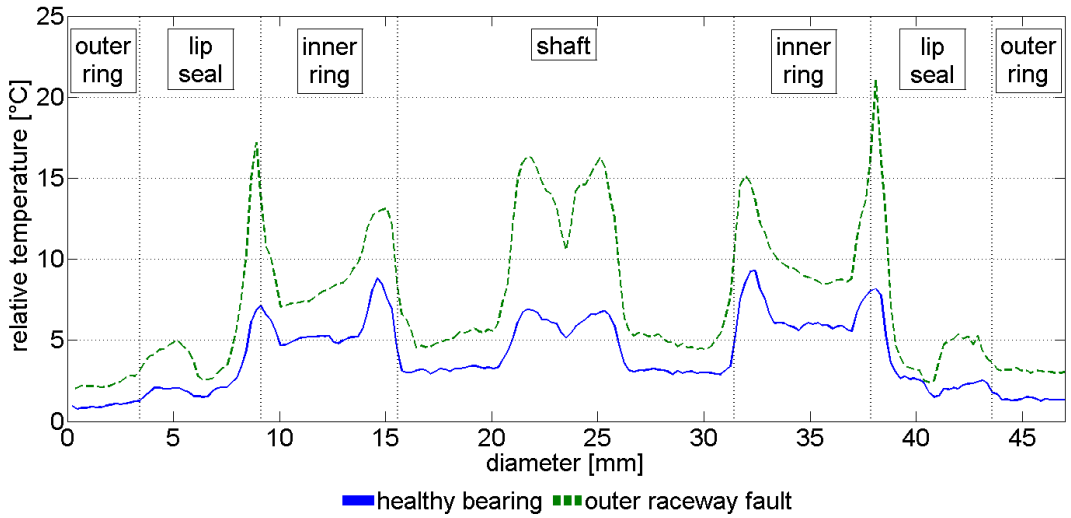

Figure 12. Hot spot temperature profiles for both healthy and faulty bearing

8. Conclusions and future work

A methodology has been proposed for processing and analysing the thermal data of healthy and faulty rolling element bearings. Different temperature rises have been monitored for both a healthy deep groove ball bearing and a bearing with outer raceway fault. With the inner ring not being covered in the used setup, it was possible to localize the outer raceway fault by means of its thermal impact on the contact surface of inner ring and rolling elements. Furthermore, the outer raceway fault leads to a faster and higher heat increase of the visible bearing parts as well as the housing part covering the outer ring in the used setup. As the fault impact could be monitored on both stationary components such as outer ring and seal as well as rotating components such as inner ring and shaft, thermal imaging shows potential for monitoring rotating machinery. The differences in heat increase on the housing can be promising for monitoring completely covered bearings in industrial applications.

As drive train components such as bearings and gearbox are usually fully covered and sealed in order to protect them from water- and hard-particle contamination, the feasibility of thermal imaging to detect faults of fully covered components has to be further examined. The higher temperatures of the bearing housing covering the faulty outer ring as well as their more rapid increase can be first indications.

References

1. M. Entezami, S. Hillmansen, C. Roberts, 'Distributed Fault Detection and Diagnosis for Wind Farms', Annual Conference of the Prognostics and Health Management Society, 2010.
2. S. Costinas, I. Diaconescu, I. Fagarasanu, 'Wind Power Plant Condition Monitoring', 3rd WSEAS International Conference on Energy Planning, Energy Saving, Environmental Education, 2009.
3. S. Sheng, 'Investigation of Various Condition Monitoring Techniques Based on a Damaged Wind Turbine Gearbox', 8th International Workshop on Structural Health Monitoring, 2011.
4. A. Hamilton, F. Quail, 'Detailed State of the Art Review for the Different Online/Inline Oil Analysis Techniques in Context of Wind Turbine Gearboxes', Journal of Tribology, Vol. 133, No. 4, 2011.
5. E.J. Terrell, W.M. Needelman and J.P. Kyle, 'Wind Turbine Tribology', Green Tribology - Biomimetics, Energy Conservation, and Sustainability, pp. 483-530, 2012.
6. Z. Daneshi-Far, G.A. Capolino, H. Henao, 'Review of Failures and Condition Monitoring in Wind Turbine Generators', XIX International Conference on Electrical Machines, 2010.
7. B. Lu, Y. Li, X. Wu, Z. Yang 'A Review of Recent Advances in Wind Turbine Condition Monitoring and Fault Diagnosis', IEEE Power Electronics and Machines in Wind Applications, 2009.
8. W. Musial, S. Butterfield, 'Improving Wind Turbine Gearbox Reliability', European Wind Energy Conference, 2007.
9. Z. Zhang, A. Verma, A. Kusiak, 'Fault Analysis and Condition Monitoring of the Wind Turbine Gearbox', IEEE Transactions on Energy Conversion, Vol. 27, No. 2, 2012.
10. S. Sheng, P. Veers, 'Wind Turbine Drivetrain Condition Monitoring - An Overview', Applied Systems Health Management Conference, 2011.
11. KOYO SEIKO CO. LTD., 'Ball and Roller Bearings - Failures, Causes, Countermeasures', 2009.
12. AB SKF, 'Bearing failures and their causes', 1994.
13. M.R. Sharlon, 'Active Thermography: An Overview of Methods and Their Applications in Use Today', IRINFO.ORG, 2008.
14. M. Cherfaoui, 'Innovative Techniques in Non-Destructive Testing and Industrial Applications on Pressure Equipment', Procedia Engineering, Vol. 46, pp. 266-278, 2011.
15. N.P. Avdelidis, B.C. Hawtin, D.P. Almond, 'Transient thermography in the assessment of defects of aircraft composites', NDT&E International, Vol. 36, pp. 433-439, 2012.
16. F.P. Garcia Marquez, A.M. Tobias, J.M. Pinar Perez, M. Papaelias, 'Condition monitoring for wind turbines: Techniques and methods', Renewable Energy, Vol. 46, pp. 169-178, 2012.
17. P.J. Tavner, 'Review of condition monitoring of rotating electrical machines', IET Electric Power Applications, Vol. 2, No. 4, pp. 215-247, 2008.
18. N. Nise, 'Control Systems Engineering', 6th edition, pp. 166-168, 2011.
19. Hannon W.M., Houpert L., 'Rolling Bearing Heat Transfer and Temperature', Encyclopedia of Tribology, pp. 2831-2839, 2013